

TOA Estimation for IR-UWB Systems with Different Transceiver Types

İsmail Güvenç, *Student Member, IEEE*, Zafer Şahinoğlu, *Member, IEEE*, and Philip Orlik, *Member, IEEE*

Abstract—In this paper, performances of stored-reference (SR), transmitted-reference (TR), and energy detection (ED) based time of arrival (TOA) estimation techniques are analyzed for impulse-radio ultra-wideband (IR-UWB) systems at sub-Nyquist sampling rates. First, an additive white Gaussian noise (AWGN) channel is considered to emphasize certain fundamental issues related to these different transceivers. In particular, energy collection characteristics and decision statistics are presented. Probability of accurate peak detection is analyzed for each transceiver; and receiver operating characteristics for the leading edge are derived. Effects of number of pulses per symbol and number of averaging symbols are investigated in detail. Then, realistic multipath channels are addressed; and various maximum likelihood estimation approaches are investigated. A new estimator that jointly exploits the noise statistics and power delay profile of the channel is proposed, and a Bayesian estimator that (ideally) gives a lower bound is analyzed. Simulation results show that while ED and TR have better energy collection capabilities at low-rate sampling, they suffer from distributing the energy over time.

I. INTRODUCTION

Ultra-wideband (UWB) is a technology that has distinct features characterized by its extremely wide bandwidth. Due to high time resolution, it is arduous but possible to accurately identify the first arriving signal component. However, the large bandwidth which is typically larger than 500MHz makes it difficult and costly to operate receivers at above the Nyquist rate. Instead, energy can be captured at lower sampling rates after certain analog front-end processing.

The energy detection (ED) of the signal is achieved by passing the signal through a square-law device, followed by an integrator and sampler. Another option is to correlate the signal with a stored-reference (SR) before an integrate-and-dump circuitry. The latter is more robust to noise effects due to the template being noise-free. In order to avoid timing and pulse-shape mismatch between the template and received signal, a transmitted-reference (TR) scheme can also be considered, where a template is transmitted with and matches the transmitted data signal with a known delay in between. After energy capturing in ED, SR and TR via low-rate digital samples, leading edge detection is needed for precision ranging. Apart from the fact that each receiver type has different captured-energy statistics, they also have different levels of susceptibilities to timing mismatches and responses to sub-Nyquist sampling.

İsmail Güvenç (iguvenc@eng.usf.edu) is a Ph.D. student in Department of Electrical Engineering, University of South Florida.

Dr. Zafer Sahinoglu (zafer@merl.com) and Dr. Philip Orlik (porlik@merl.com) are with the Mitsubishi Electric Research Labs, Cambridge, MA.

Typical approaches for UWB time of arrival (TOA) estimation in the literature are based on Nyquist rate (or near Nyquist rate) sampling of signals [1], [2], using an SR [3], [4], and an ED [4], [5] receivers. A coarse timing estimate of a signal can be achieved by maximum energy selection (MES) [3], [5], [6]-[10]. Some other detection related work in the literature includes [11], where detection performances of IR-UWB signals with a square law device were investigated, and [12], where receiver operating characteristics (ROCs) for coherent UWB random noise radars have been analyzed. Detection performances of weighted square-law and cross-correlation UWB receivers are analyzed in [13]. In [14], an in-depth analysis of signal acquisition using matched filtering and ED is carried out. Acquisition is achieved using a generalized likelihood ratio testing (GLRT) and noisy templates in [15], [16]. On the other hand, a coherent acquisition scheme with low-rate samples is discussed in [17], which shows that the complexity can be reduced by sub-sampling. Once an initial acquisition is achieved, precise arrival of the leading edge can be estimated by various thresholding techniques [1], [18], [19]. Trade-offs between SR and TR transceiver types for symbol detection are addressed in [20].

The performance trade-offs and comparison of different transceiver types for UWB timing estimation is not available in the literature to the best knowledge of the authors. In this paper, SR, TR, and ED based receivers and timing estimation schemes operating at sub-Nyquist rates are analyzed and compared. Our contributions are as follows. First, with the assumption of additive white Gaussian noise (AWGN) channels, statistics and energy collection characteristics of the three transceiver types are addressed. Then, peak selection error, leading edge detection error (conditioned on the energy capture characteristics of the transceivers at low-rate sampling), and effects of pulse compression (increasing the number of pulses per symbol) and processing gain achievable from replicate symbol transmissions are discussed. Afterwards, the TOA estimation performance is analyzed under multipath channels via likelihood based estimators. A Bayesian estimator algorithm that ideally gives a lower bound is presented.

II. SYSTEM MODEL

While the transmitted signal structures are the same for SR and ED receivers, TR includes delayed version of the same signal, and therefore yielding a slightly different transmitted signal model. Let the received UWB signal in multipath

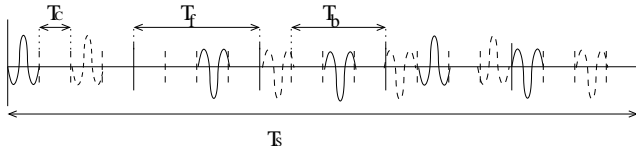


Fig. 1. Illustration of IR-UWB pulse transmissions in a symbol, where $(N_s, N_h) = (5, 4)$, $T_b = 3T_c$, and $(\{c_j\}, \{d_j\}) = (\{0, 2, 1, 1, 0\}, \{+1, -1, -1, +1, -1\})$. The pulses with solid lines correspond to ED and SR. Dashed pulses can be included for TR (after appropriate energy scaling) with $D = 2T_c$.

channel for the former schemes be represented as

$$r(t) = \underbrace{\sum_{j=-\infty}^{\infty} d_j \omega_{mp}(t - jT_f - c_j T_c - \tau_{toa})}_{r_s(t)} + n(t), \quad (1)$$

while for the TR case the received signal is modeled by

$$\tilde{r}(t) = \frac{1}{\sqrt{2}}(r_s(t) + r_s(t - D)) + n(t), \quad (2)$$

where frame index and frame duration are denoted by j and T_f , T_c is the chip duration, T_s is the symbol duration, and τ_{toa} is the TOA of the received signal. Effective pulse after channel effects is given by $\omega_{mp}(t) = \sqrt{\frac{E_b}{N_s}} \sum_{l=1}^L \alpha_l \omega_l(t - \tau_l)$, where $\omega_l(t)$ is the received UWB pulse at l th tap with unit energy, E_b is the symbol energy (we assume N_s pulses per symbol), α_l and τ_l are the fading coefficients and delays of the multipath components, respectively, and $\sum_{l=1}^L \alpha_l^2 = 1$. The AWGN with zero-mean and double-sided power spectral density $N_0/2$ and variance σ^2 is denoted by $n(t)$. The delay between the data and reference signals¹ is denoted by D , and energy is appropriately scaled so that energy per symbol is identical for all cases. No modulation is considered for the ranging process. In order to avoid catastrophic collisions (large number of hits between the pulses of different users), and smooth the power spectral density of the transmitted signal, time-hopping codes $c_j \in \{0, 1, \dots, N_h - 1\}$ are assigned to different users, with $N_h = T_f/T_c$ denoting the number of chip positions per frame. Moreover, random-polarity codes $d_j \in \{\pm 1\}$ are used to get additional processing gain for the detection of desired signal, and smooth the signal spectrum (see Fig. 1).

A. Sampling the Received Signal After Different Energy Collection Techniques

The signal arriving at the receiver's antenna is passed through a low noise amplifier (LNA) and a band pass filter (BPF) of bandwidth B . Different approaches for collecting the energy are possible before sampling the signal in (1) or (2). The received signal can be sampled after correlation with a stored-reference signal (Fig. 2a), after correlation with a transmitted-reference signal (Fig. 2b), or after a square-law device (Fig. 2c). Block duration (which corresponds to the sampling interval) is denoted by T_b , and is equivalent to T_c

¹Even though we refer the pair of signals in TR as reference and data signals, this is just for the sake of distinction, and we consider no data modulation for ranging purposes.

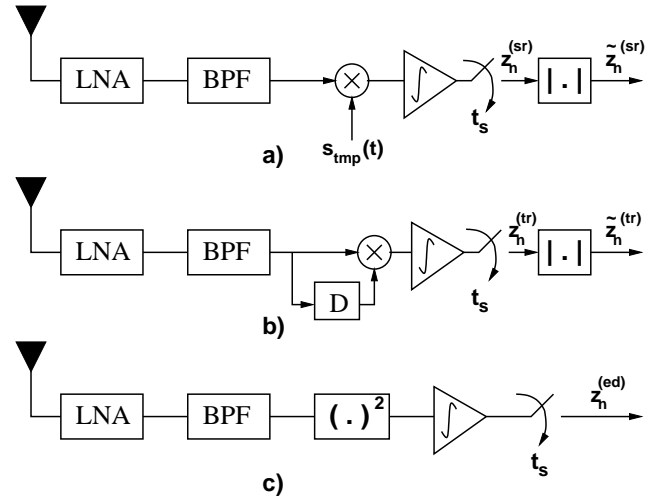


Fig. 2. Sampling of the received signal after a) Correlation with a local reference, b) Correlation with a transmitted reference, and c) Energy detection.

for chip-spaced sampling. In the sequel, we assume that a coarse acquisition on the order of frame-length is acquired, such that in (1) $\tau_{toa} \sim \mathcal{U}(0, T_f)$, where $\mathcal{U}(\cdot)$ denotes the (continuous) uniform distribution. The block index that contains the first arriving signal energy is corresponded by $n_{toa} \in \{1, 2, \dots, N_{toa}\}$, where $N_{toa} = \frac{T_f}{T_b}$. The signal within time frame T_f plus half of the next frame is sampled and searched to factor-in inter-frame leakage due to multipath. Thus, the number of samples (or blocks/chips) within the TOA search region is given by $N_b = \frac{3}{2} \frac{T_f}{T_b}$, and $n \in \{1, 2, \dots, n_{toa}, \dots, N_b\}$ denotes the sample index with respect to the starting point of the uncertainty region.

With a sampling interval of t_s , the SR template signal and the samples collected after correlating the received signal with this template are given by,

$$s_{tmp}(t) = \sum_{j=0}^{N_s-1} d_j \omega(t - jT_f - c_j T_c), \quad (3)$$

$$z_n^{(sr)} = \int_{(n-1)t_s}^{(n-1)t_s + N_s T_f} r(t) s_{tmp}(t - (n-1)t_s) dt, \quad (4)$$

respectively, where ω denotes the correlator pulse shape². Since no channel estimate is available prior to signal acquisition and TOA estimation, absolute values of SR outputs are used (as shown in Fig. 2), yielding $\tilde{z}_n^{(sr)} = |z_n^{(sr)}|$.

The samples at the output of the square-law device are

$$z_n^{(ed)} = \sum_{j=1}^{N_s} \int_{(j-1)T_f + (c_j + n-1)t_s}^{(j-1)T_f + (c_j + n)t_s} |r(t)|^2 dt, \quad (5)$$

while the samples after correlating with the delayed version

²Note that since received pulse shape ω_l can change at different multipath components due to its large bandwidth, ω will not typically match with the received pulse shapes. However, we have used $\omega = \omega_l$ for all l in the simulations for simplicity.

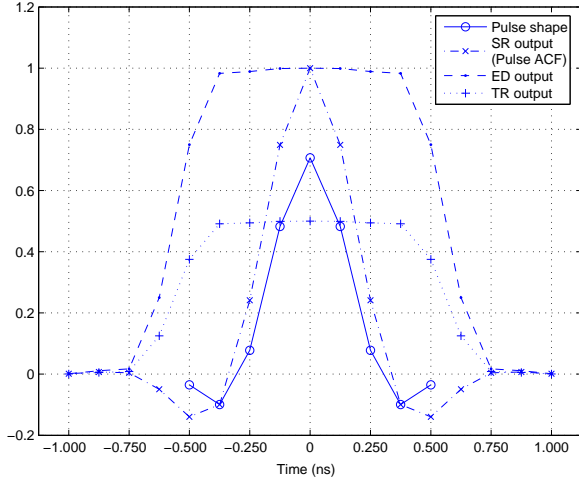


Fig. 3. Received *normalized* pulse shape, and the sampled outputs corresponding to SR, ED, and TR for different timing offsets (1ns pulse is sampled at 8GHz, and energy is collected within 1ns windows and different time offsets).

of the signal itself is formulated as

$$z_n^{(tr)} = \sum_{j=1}^{N_s} \int_{(j-1)T_f + (c_j+n-1)t_s}^{(j-1)T_f + (c_j+n)t_s} \tilde{r}(t) \tilde{r}(t - D) dt. \quad (6)$$

In the TR case as well, the absolute values of the samples are used to yield $\hat{z}_n^{(tr)} = |z_n^{(tr)}|$. The performance can be further improved by having a processing gain from multiple symbol transmissions. Note that averaging must be performed prior to absolute-value operation. In what follows, we refer to the number of symbols as N_{sym} .

B. Trade-offs Between Different Transceiver Architectures

It is very well known that matched filtering, in which a stored reference template is correlated with the received signal, is optimal detection technique when the knowledge of the received waveform shape is available. However, Nyquist-rate sampling is essential to match with the received signal, so that perfect alignment with the template and received waveform can be obtained. If only lower sampling rates are possible, it is apparent from (4) that the SR will not be able to collect sufficient energy from the received multipath arrivals due to timing mismatches (and pulse shape distortions).

On the other hand, ED and TR signaling can both effectively capture the received energy. Even at sub-Nyquist sampling rates, neither scheme requires the knowledge of the sampling timing or pulse shapes (assuming accurate delay lines for the TR case). The existence of the TR pulse yields a 3dB transmitted energy loss compared with the other two schemes. Illustration of the timing susceptibility for SR, TR, and ED are presented in Fig. 3. If a sufficient sampling rate is available, the SR will better characterize the peak; however, at low sampling rates (e.g. $t_s > 1$ ns), it becomes more likely for SR to miss the peak.

Note that in non-coherent approaches the enhanced noise terms in the low SNR region becomes an issue. In particular,

noise-square terms for the ED, and noise-cross-noise terms for TR seriously dominate and degrade the detection performance. Therefore, even though a non-coherent approach outperforms the SR at high SNR due to better energy capture at sub-Nyquist sampling rates, they have poor performance when the noise variance is large. Moreover, non-coherent schemes suffer from degraded SNR when symbol energy is spread over more pulses, whereas energy in an SR symbol can be distributed over multiple pulses with no SNR loss. Due to similar reasons, TR and ED are much more susceptible to interference compared to SR. A cross-correlation receiver can also be considered instead of TR (as in [13]), which yields identical energy capture with ED but a smaller noise variance.

Comparing the transmitted waveforms, TR has a longer time span compared to ED and SR, and D has to be large enough so that multipath interference between reference and data pulses is not a serious problem. Also, TR observes enhanced early/late (E/L) noise terms that arise when either the reference or data signal samples are correlated with the noise-only samples. This scales the noise variance at $\pm D$ of the actual TOA by the signal energy. Finally, the delayed signal from a previous frame may affect the results for TR receivers, and D parameter should be selected carefully considering the frame duration and the maximum excess delay of the channel.

In the next sections, first, an AWGN channel is considered to highlight certain points related to different transceiver types. Some of the fundamental trade-offs discussed in this section are expanded in detail. Later, under realistic multipath channel models, maximum likelihood techniques for time of arrival estimation are given.

III. AWGN CHANNEL ANALYSIS

UWB receivers typically observe dispersive channels that have hundreds of multipath components. However, it is more useful to analyze certain fundamental aspects related to signal acquisition and leading edge detection in less complicated scenarios. In this section, we consider an AWGN channel ($L = 1$, $\alpha_1 = 1$, $\tau_1 = 0$), and analyze performance trade-offs between different transceiver types. In particular, decision statistics (for single and multiple pulses per symbol), as well as energy collection characteristics under timing mismatch (due to sub-Nyquist sampling) are investigated in detail. Peak selection performances are compared for the three schemes, which is closely tied with signal acquisition. Then, leading edge detection characteristics are analyzed by conditioning the detection probability on the leading edge energy, which depends on the transceiver's energy collection capability.

A. Decision Statistics

As in any detection or estimation problem, the performance depends on decision statistics, which are derived from $z_n^{(ed)}$, $z_n^{(tr)}$, and $z_n^{(sr)}$ for the problem in hand (prior to any absolute value operation for SR and TR). Due to nature of the acquisition and leading edge estimation problem, no parameter estimates (i.e., the channel estimate) are available to the receiver, which makes the receiver strictly sub-optimal [14]. Below, we assume a Gaussian approximation of the signal

TABLE I
COMPARISON OF OUTPUT STATISTICS FOR DIFFERENT TRANSCIEVER
TYPES.

| | SR | TR | ED |
|-----------------|---|--|---|
| μ_{no} | 0 | 0 | $N_s M \sigma^2$ |
| σ_{no}^2 | $\frac{N_s \sigma^2}{N_{sym}}$ | $\frac{N_s M \sigma^4 + \sigma^2 \frac{E_b}{2}}{N_{sym}}$ | $\frac{2N_s M \sigma^4}{N_{sym}}$ |
| μ_{sn} | $N_s \sqrt{\frac{E_b}{N_s}} = \sqrt{N_s E_b}$ | $E_b/2$ | $N_s M \sigma^2 + E_b$ |
| σ_{sn}^2 | $\frac{N_s \sigma^2}{N_{sym}}$ | $\frac{N_s M \sigma^4 + 2\sigma^2 \frac{E_b}{2}}{N_{sym}}$ | $\frac{2N_s M \sigma^4 + 4\sigma^2 E_b}{N_{sym}}$ |

statistics for TR and ED, which is valid for large $M \times N_s$ and becomes more accurate if the signal is averaged over large number of symbols. M denotes the degree of freedom of the noise such that $M = 2Bt_s + 1$.

Consider a scenario where ideal sampling instants are assumed, and $t_s = T_c$. Using a normalized template at the receiver, the output of the correlator is given by $\sqrt{E_b}$ in the presence of signal, and the noise variance is given by σ^2 regardless of the presence of the signal. On the other hand, the captured signal energy is E_b for ED, and $E_b/2$ for TR (due to reference pulse). The arising noise-cross-noise terms and noise-square terms enhance the noise variance in TR and ED, respectively. Note that before any absolute-value operation, ED is the only scheme that has a non-zero noise-mean (but also has a larger energy *offset* compared to the others). When N_s pulses per symbol are used, and/or the samples are averaged over N_{sym} symbols, the statistics can be easily shown to yield the values in Table I, where notations (no) and (sn) correspond to noise-only and signal-plus-noise cases³.

After the samples of SR and TR are fed into the absolute value operator, their statistics obviously change. However, their distributions can be still derived in terms of the statistics of the original Gaussian parameters. In the presence of signal, the distribution of $\tilde{z}_{sn} = |z_{sn}|$ (i.e. the absolute values of the samples for SR and TR as illustrated in Fig. 2) can be easily formulated as⁴

$$p(\tilde{z}_{sn}) = \begin{cases} 0 & \text{if } z_{sn} < 0, \\ \frac{1}{\sqrt{2\pi\sigma_{sn}^2}} \left[\exp\left(-\frac{(z_{sn}-\mu_{sn})^2}{2\sigma_{sn}^2}\right) + \exp\left(-\frac{(-z_{sn}-\mu_{sn})^2}{2\sigma_{sn}^2}\right) \right] & \text{if } z_{sn} \geq 0, \end{cases} \quad (7)$$

which for $\mu_{sn} \rightarrow 0$ becomes the special case for noise-only samples

$$p(\tilde{z}_{no}) = \begin{cases} 0 & \text{if } z_{no} < 0, \\ \frac{2}{\sqrt{2\pi\sigma_{no}^2}} \exp\left(-\frac{z_{no}^2}{2\sigma_{no}^2}\right) & \text{if } z_{no} \geq 0, \end{cases} \quad (8)$$

and above formulations still allow using Q-functions to evaluate the detection errors. Note that if SNR is large, as an approximation, the second exponential term in (7) may be neglected (since the area under the tail will be negligible).

³For the rest of the paper, we neglect the effects of time-hopping and polarity randomization codes (i.e. $c_j = 0$ and $d_j = 1$ for all j) for the simplicity of analysis.

⁴See [21] for calculating the probability density function (PDF) of a function of a random variable.

B. Peak Selection Error

Acquisition of an UWB radio signal is commonly achieved by peak selection of the received signal samples, which gives a coarse TOA information. The leading edge detection can then be performed using different search-back schemes. Considering a single-tap channel and alignment of the sampling instants with chips, the probability of peak selection can be formulated as (z_n denotes any of $z_n^{(ed)}$, $\tilde{z}_n^{(sr)}$, or $\tilde{z}_n^{(tr)}$)

$$\begin{aligned} P_{ps} &= P(\hat{n} = n_{max}) \\ &= \int_{z_{n_{max}}=0}^{\infty} P(z_1 < z_{n_{max}}) P(z_2 < z_{n_{max}}) \times \dots \\ &\quad \times p(z_{n_{max}}) P(z_{n_{max}+1} < z_{n_{max}}) \times \dots \\ &\quad \times P(z_{N_b} < z_{n_{max}}) dz_{n_{max}}, \end{aligned} \quad (9)$$

where $n_{toa} = n_{max}$ denotes the location of the peak. After some manipulation, (9) yields

$$P_{ps} = \int_{z_{n_{max}}=0}^{\infty} \left(1 - \mathcal{K}Q\left(\frac{z_{n_{max}} - \mu_{no}}{\sigma_{no}}\right)\right)^{N_b-1} p(z_{n_{max}}) dz_{n_{max}}, \quad (10)$$

where $z_{n_{max}} \sim \mathcal{N}(\mu_{sn}, \sigma_{sn}^2)$, $\mathcal{K} = 1$ for ED and $\mathcal{K} = 2$ for SR or TR. Note that the second exponential in (7) is neglected for simplicity, which yields a good approximation as will be compared later with the simulations. The probability of erroneously selecting a noise-only sample as the peak is then given by

$$P_{pse} = 1 - P_{ps}. \quad (11)$$

C. Leading Edge Detection and Effects of Non-Ideal Sampling Instant

If sampling instants are aligned with chip positions, sampling the received signal at chip-rate would be sufficient to capture the correlation peaks. However, due to lack of synchronization the received signal may arrive anywhere within the sampling block. Therefore, how finely the correlation peaks (and the leading edge) are characterized depends on the sampling rate of the received signal, as well as receiver's energy output characteristics. In Fig. 3, the pulse shape used in this paper (root raised cosine pulse), and the energy outputs of the SR, TR, and ED are shown. For a uniformly distributed TOA, each of the samples become equally likely to be the leading edge sample, and the PDFs and cumulative distribution function (CDFs) of the leading edge energy sample (i.e., E_{le}) can be easily obtained for different transceivers.

In order to analyze the leading edge detection performance of different transceiver types in AWGN channels, consider a 1-tap channel and chip-spaced sampling, where the pulse duration is equal to the chip interval. Then, the received pulse may arrive anywhere within the first energy block, implying that an energy sample may contain only a fraction of the entire pulse energy. As discussed before, the PDF of this fractional energy will change for different transceiver types. Using Neyman-Pearson theory, the threshold that maximizes the detection probability can be found for a given false-alarm probability. In the absence of the signal, the false alarm

probability can be defined as the probability of erroneously selecting the noise-only sample as a signal-containing sample, and is given by

$$P_{fa} = \mathcal{K}Q\left(\frac{\xi - \mu_{no}}{\sigma_{no}}\right), \quad (12)$$

and for a fixed P_{fa} , the threshold is given by

$$\xi = \sigma_{no}Q^{-1}\left(\frac{P_{fa}}{\mathcal{K}}\right) + \mu_{no}. \quad (13)$$

Given the threshold for a particular P_{fa} , the detection probability of the leading edge can be obtained for different transceivers by averaging over the PDF of E_{le} . For a multipath channel, the detection probability of the leading edge can be defined to be probability of accurate detection of the leading edge after searching back the samples prior to the maximum energy sample. However, due to cumbersome channel statistics caused by multiple clusters and delay spread, and diversity of acquisition and leading edge detection techniques, such an analysis is not followed in this paper. Instead, we define the probability of detection for the leading edge as

$$P_D = \int_0^\infty P(z_{le} > \xi)p(E_{le})dE_{le}, \quad (14)$$

where $P(z_{le} > \xi)$ using (7) is given by (assuming ED has a large noise offset)

$$P(z_{le} > \xi) = \begin{cases} 1 - Q\left(\frac{\mu_{le} - \xi}{\sigma_{le}}\right) + Q\left(\frac{\mu_{le} + \xi}{\sigma_{le}}\right) & \text{if SR or TR,} \\ 1 - Q\left(\frac{\mu_{le} - \xi}{\sigma_{le}}\right) & \text{if ED,} \end{cases} \quad (15)$$

E_{le} is the instantaneous leading edge energy, whose PDF can be obtained from the correlation functions of the three different transceiver types (Figs. 3), and μ_{le}, σ_{le} are the mean and the standard deviation of the leading edge energy sample, respectively. Regardless of the leading edge search scheme after acquisition, (14) characterizes how likely we can detect the leading edge once/if we reach it.

IV. MULTIPATH CHANNEL ANALYSIS AND LIKELIHOOD BASED TOA ESTIMATION

In realistic multipath channels, the detection performance of the leading edge defined in previous section is not the only measure of the timing estimation error, and channel statistics such as the number of clusters, delay between the peak and the leading edge etc. should be taken into consideration [9], [22]. Since there may be a large delay between the peak and the leading edge, typically, any of the samples that arrive later (or earlier, depending on the algorithm) than the leading edge may be selected as the TOA, and thus closed form theoretical error expressions are non-trivial due to cumbersome channel characteristics.

In order to illustrate the timing difference between the strongest sample and the leading edge sample, consider the CM1 channel model in [23]. The CDF of the delays between the maximum energy sample and the leading edge sample for this channel model are compared for different transceiver types in Fig. 4 with and without path offset within the first energy

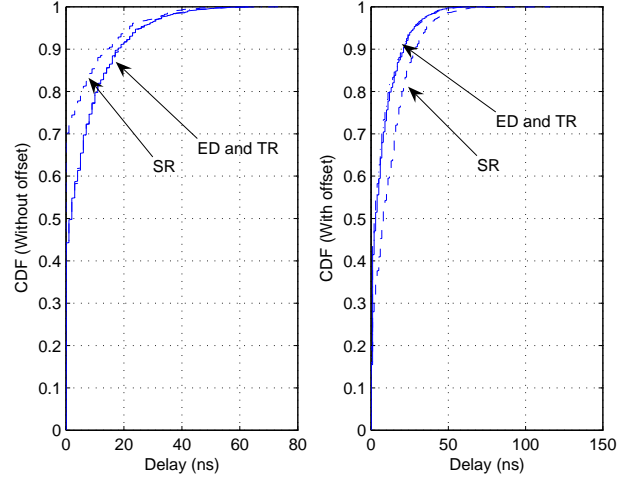


Fig. 4. CDFs of delays between peak and leading edge for SR, TR, ED ($t_s = T_b = 1$ ns), and with and without path offsets within first energy block.

block⁵. While choosing the peaks yields a closer timing to the leading edge for SR in the first scenario, ED and TR has better characteristics at low sampling rates when no first-path synchronization is assumed.

Due to this large possible delay between the peak and the leading edge, peak selection fails to give accurate timing estimates, and more sophisticated algorithms are required. In this section, rather than threshold based techniques as in [18], [19], [22], we consider likelihood based estimation of the signal timing. Starting from a simple peak selection that discards the energy information in the neighboring samples, maximum likelihood methods of different complexity levels (and *a-priori* information requirements) will be analyzed. Since the location of the peak is assumed unknown, the techniques to be discussed may also be used for initial signal acquisition.

A. Problem Formulation

Let \underline{z} denote⁶ the $1 \times N_b$ vector of samples z_n , N_e denote the number of signal plus noise energy samples, $\underline{z}_k^{(no)}$ and $\underline{z}_k^{(sn)}$ denote (for the k th hypothesis) the noise-only energy vector and signal plus noise energy vector of sizes $1 \times (N_b - N_e)$ and $1 \times N_e$, respectively, where vectors on the two sides of signal plus noise vector $\underline{z}_k^{(sn)}$ are concatenated to yield $\underline{z}_k^{(no)}$. Consider an ED with $N_s = 1$. Then, the following multiple hypothesis testing can be formulated for $k = 1, 2, \dots, N_{toa}$

$$\mathcal{H}_k : \begin{cases} z_n = \int_{(n-1)T_b}^{nT_b} \eta^2(t)dt, & n = 1, \dots, k-1 \\ z_n = \int_{(n-1)T_b}^{nT_b} [r_s(t) + \eta(t)]^2 dt, & n = k, \dots, k + N_e - 1 \\ z_n = \int_{(n-1)T_b}^{nT_b} \eta^2(t)dt, & n = k + N_e, \dots, N_b \end{cases} \quad (16)$$

⁵We define the path offset to be the relative time difference between the first arriving path and the beginning of the leading edge block. As implied by the discussion in Section II-A, it is assumed uniformly distributed.

⁶The samples z_n in the sequel correspond to $z_n^{(ed)}$. However, similar analysis may also be easily performed for z_n being $z_n^{(sr)}$ and $z_n^{(tr)}$.

where $\eta(t)$ is the noise after the BPF (signal part is assumed to be undistorted due to BPF), and $\mathcal{H}_{n_{toa}}$ is the correct hypothesis. Note that maximum likelihood estimation of the correct hypothesis requires the channel statistics and the noise variance information.

Using the Chi-square statistics [24] that arise due to the square-law device, (16) becomes

$$\mathcal{H}_k : \begin{aligned} z_n &= \chi(M), & n &= 1, \dots, k-1 \\ z_n &= \chi(E_n, M), & n &= k, \dots, k+N_e-1 \\ z_n &= \chi(M), & n &= k+N_e, \dots, N_b \end{aligned} \quad (17)$$

where Chi-square random variable is denoted with χ , with parameter M for the centralized, and parameters (E_n, M) for non-centralized cases, respectively. The signal energy in the n th block is denoted by E_n .

For notational convenience, define index $m \in \{1, 2, \dots, N_e\}$ for the signal plus noise energy vector for the range of $k \leq n \leq k+N_e-1$, where $m = n - k + 1$, and $\mathcal{E}_m = E_n$. Gaussian approximation can be used to model z_n for large enough M , where the means and variances become $\mu_n = M\sigma^2$, $\sigma_n^2 = 2M\sigma^4$ for the centralized, and $\mu_n = M\sigma^2 + E_n$, $\sigma_n^2 = 2M\sigma^4 + 4\sigma^2 E_n$ for the non-centralized Chi-square distributions.

B. Maximum Likelihood Estimation

Typically, N_e in (16) is much larger than 1 for T_b values on the order of pulse duration, and the signal energy is spread over many blocks. The coarsest way of obtaining a time of arrival estimate is the maximum energy selection (MES) from the individual energy samples by neglecting the information in the neighboring samples, which yields

$$\hat{n}_{toa}^{(mes)} = \operatorname{argmax}_{k \in \{1, \dots, N_b\}} \{z_k\}. \quad (18)$$

However, MES is susceptible to noise since the energy in only a single sample is used, and it does not provide high timing resolution as there may be a large delay between the leading edge and the maximum energy block (see Fig. 4).

In order to exploit the energy in the neighboring multipath components, energy samples can be summed within a window. With a window duration of $N_w \leq N_e$ blocks, the leading block estimate using maximum energy sum selection (MESS) is given by

$$\hat{n}_{toa}^{(mess)} = \operatorname{argmax}_{k \in \{1, \dots, N_b\}} \left\{ \underline{z}_k^{(sn, N_w)} \times \underline{1}_{N_w} \right\}, \quad (19)$$

where $\underline{1}_{N_w}$ is a column vector of ones of length N_w , and MESS collapses to MES for $N_w = 1$. The vector $\underline{z}_k^{(sn, N_w)}$ is composed of first N_w elements of $\underline{z}_k^{(sn)}$. Since a very large window length captures a lot of noise and small window length does not capture sufficient energy, there exists an optimum window length that changes with the channel model and the E_b/N_0 , which we will demonstrate using simulations. Note that (19) is similar conceptually to the synchronization algorithm in [5] except the window definitions and signaling schemes ([5] uses a direct-sequence UWB signaling). However, the optimality of the window length was not investigated before to our best knowledge.

If *a-priori* knowledge about the channel power delay profile is available, we propose to use it to weigh the hypothesized energy vector, which yields

$$\hat{n}_{toa}^{(wmess)} = \operatorname{argmax}_{k \in \{1, \dots, N_b\}} \left\{ \underline{z}_k^{(sn, N_e)} \times \underline{\rho}_{N_e} \right\}, \quad (20)$$

where $\underline{\rho}_{N_e}$ is the column vector of $1 \times N_e$ mean energies for a particular channel model and block duration. In [9], mean energies with respect to block index have been presented for CM1 and CM2, and for $T_b = 4\text{ns}$, which we also use for our simulations. Note that the weighted-MESS (W-MESS) in (20) is actually equivalent to correlating the received energy vector with the mean energy values before peak selection.

Careful observation of (16) shows that for correct \mathcal{H}_k , the noise parameters $\hat{\mu}_k^{(no)}$ and $\hat{\sigma}_k^{(no)}$ are minimized. Therefore, weighing the energy sum in (20) with the inverse of $\hat{\mu}_k^{(no)} \times \hat{\sigma}_k^{(no)}$ (referred to as W₂-MESS) will increase the likelihood of the correct hypothesis. The proposed TOA estimate for W₂-MESS then becomes

$$\hat{n}_{toa}^{(w_2mess)} = \operatorname{argmax}_{k \in \{1, \dots, N_b\}} \left\{ \frac{\underline{z}_k^{(sn, N_e)} \times \underline{\rho}_{N_e}}{\hat{\mu}_k^{(no)} \times \hat{\sigma}_k^{(no)}} \right\}. \quad (21)$$

Note that for both W-MESS and W₂-MESS, even if the power delay profile is not exactly available, an appropriate exponential can be used to weight the energy vector to enhance the performance of the MES.

C. Bayesian Estimation

The techniques discussed in the previous section assume the knowledge of the power delay profile, which is the average energy within individual blocks. If the distribution of \mathcal{E}_m are known *a-priori* for each energy block m , and noise variance σ^2 is known accurately (both of which are extremely difficult in most cases), an *optimal* solution can be developed using a Bayesian approach (see [25] for a discussion on Bayesian estimators). We then estimate the leading energy block as follows

$$\hat{n}_{toa}^{(Bys)} = \operatorname{argmax}_{k \in \{1, \dots, N_b\}} \left\{ \int_{\mathcal{E}_1} \int_{\mathcal{E}_2} \dots \int_{\mathcal{E}_{N_e}} p(\underline{z} | k, \sigma^2, \underline{\mathcal{E}}) \times p(\mathcal{E}_1) \dots p(\mathcal{E}_{N_e}) d\mathcal{E}_{N_e} \dots d\mathcal{E}_1 \right\}, \quad (22)$$

where $\underline{\mathcal{E}} = [\mathcal{E}_1, \mathcal{E}_2, \dots, \mathcal{E}_{N_e}]$ is the vector of signal energies in the signal plus noise blocks, the distribution function is given by (which can be simplified further)

$$\begin{aligned} p(\underline{z} | k, \sigma^2, \underline{\mathcal{E}}) &= \prod_{n=1}^{k-1} \frac{1}{\sqrt{2\pi\sigma_{no}^2}} \exp\left(-\frac{(z_n - \mu_{no})^2}{2\sigma_{no}^2}\right) \\ &\times \prod_{n=k}^{k+N_e-1} \frac{1}{\sqrt{2\pi\sigma_{sn,m}^2}} \exp\left(-\frac{(z_n - \mu_{sn,m})^2}{2\sigma_{sn,m}^2}\right) \\ &\times \prod_{n=k+N_e}^{N_{toa}} \frac{1}{\sqrt{2\pi\sigma_{no}^2}} \exp\left(-\frac{(z_n - \mu_{no})^2}{2\sigma_{no}^2}\right), \end{aligned} \quad (23)$$

where $m = n - k + 1$, and the noise-only parameters (μ_{no}, σ_{no}) and signal plus noise parameters at the m th energy sample $(\mu_{sn,m}, \sigma_{sn,m})$ are calculated from Table I using $\underline{\mathcal{E}}$ and σ . The PDFs of elements of $\underline{\mathcal{E}}$ within 100 discrete bins in $(0, 1)$ are presented in [9], which we also use in the simulations, and do not repeat here due to space limitations. It is desirable to choose N_e on the order of maximum excess delay to have accurate estimates.

Note that in order to keep the problem analytically tractable, (22) assumes that the energies \mathcal{E}_m are uncorrelated. The ideal Bayesian estimator should consider the joint PDFs of the energies, which is very difficult to extract from the channel models.

Since it is usually very hard to know the prior PDFs of the parameters, and it requires multidimensional integration over the PDF of each parameter yielding a very complex implementation, Bayesian analysis is usually of theoretical interest and serves as a benchmark for other sub-optimal estimators rather than for practical consideration.

V. NUMERICAL RESULTS

Computer simulations are performed to compare detection performances of different transceiver types in AWGN and in multipath channels. A raised cosine pulse of $T_c = 1$ ns is considered for all scenarios, and the received signal is sampled at 1ns for AWGN channel, and 1ns or 4ns for multipath channels. The delay D is set to 60ns for TR.

For AWGN channel simulations, peak selection performances and ROCs of the different transceiver types are analyzed for various N_b , N_s , and N_{sym} with and without perfect alignment of sampling instants to chip intervals.

In multipath scenarios, the channel models CM1 (residential LOS) and CM2 (residential NLOS) of IEEE802.15.4a are used. The channel realizations are sampled at 8GHz, 1000 different realizations are generated, and each realization has a TOA uniformly distributed within $(0, T_f)$. After introducing uniformly distributed delays (first path may arrive anywhere within the first signal block), energies are collected within non-overlapping windows to obtain decision statistics. The other simulation parameters are $T_f = 200$ ns, $B = 4$ GHz⁷, $N_s = 1$, and only a single ranging symbol is used. Both 1ns and 4ns are considered for T_b , with corresponding N_e of 100 and 25, respectively, so that significant multipath energy can be captured. For all the simulations the TOA estimate is taken to be the center of the block estimate, and timing errors are averaged over 1000 different channel realizations.

A. AWGN Channel Simulations

1) *Peak Selection Error*: In Fig. 5, theoretical peak selection errors are compared for different settings of N_s (to be compared with simulations in Fig. 6). For perfect synchronization, SR outperforms the other transceiver types. Moreover, SR is not affected from increasing number of pulses per symbol, while ED and TR performances seriously degrade

⁷Note that for a sampling interval $t_s = 1$ ns, the sampling rate corresponds to 1/8 of the required Nyquist rate.

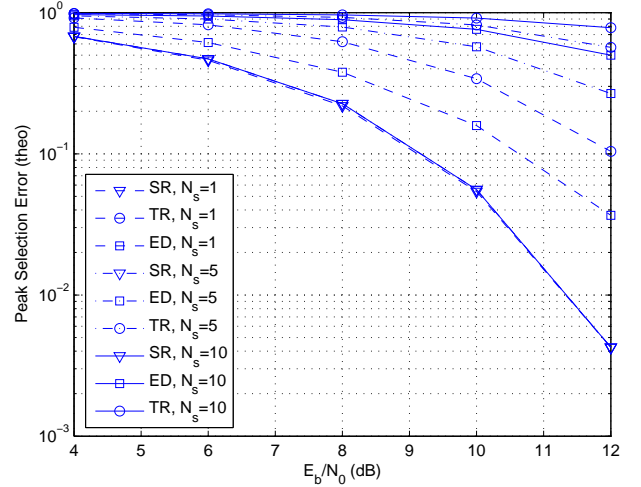


Fig. 5. Peak selection errors (theory) of different transceiver types for AWGN channel and for different N_s ($N_b = 100$, $N_{sym} = 1$, $M = 8$).

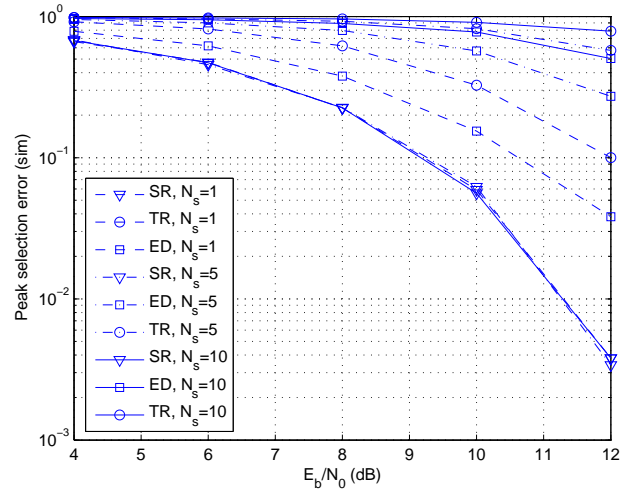


Fig. 6. Peak selection errors (simulation) of different transceiver types for AWGN channel and for different N_s ($N_b = 100$, $N_{sym} = 1$, $M = 8$).

with increasing N_s (as also implied by Table I). Effects of N_{sym} on peak selection error are presented in Fig. 7, where SR is seen to better benefit from the processing gain.

2) *Leading Edge Detection Simulation Results*: In order to assess the leading edge detection performances, a uniformly distributed τ_{toa} is considered, and the detection performance of the leading edge is analyzed. In Fig. 8, theoretical ROCs (P_D vs. P_{fa}) of different transceiver types are shown for two different E_b/N_0 values (see Fig. 9 for the simulation results). While SR performed well for peak selection with perfect synchronization (in previous figures), its ROC is worse than the other two transceivers when timing mismatches are considered. This is due to the energy collection characteristics of different transceivers. Note that ROC is the worst for the 45° line, which may be obtained using a detector that ignores all the data (i.e., by tossing a coin) [25]. When $N_s > 1$, as expected, the performance of SR is not affected, and

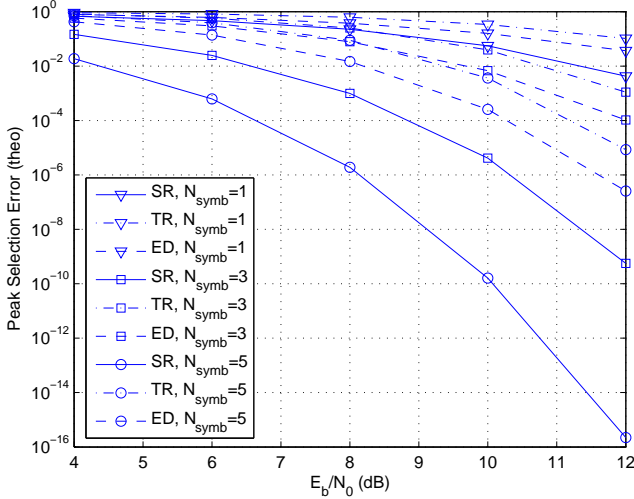


Fig. 7. Peak selection errors (theory) of different transceiver types for $N_{\text{symb}} = 1, 3, 5$ ($N_b = 100$, $N_s = 1$, $M = 8$).

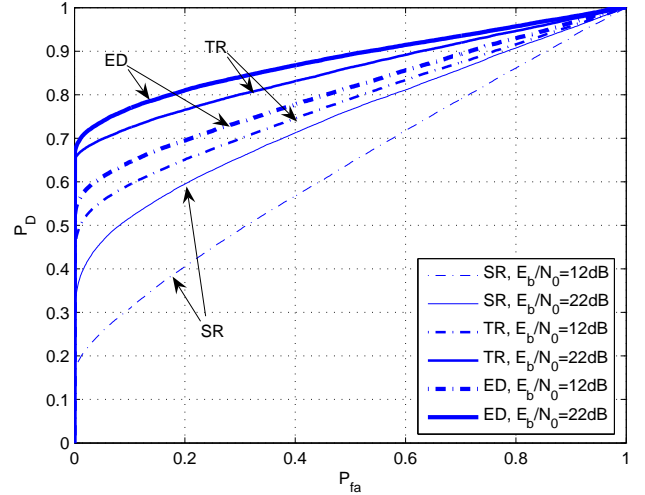


Fig. 9. ROC (simulations) for different transceiver types and in the presence of timing offsets ($N_s = 1$, $M = 8$).

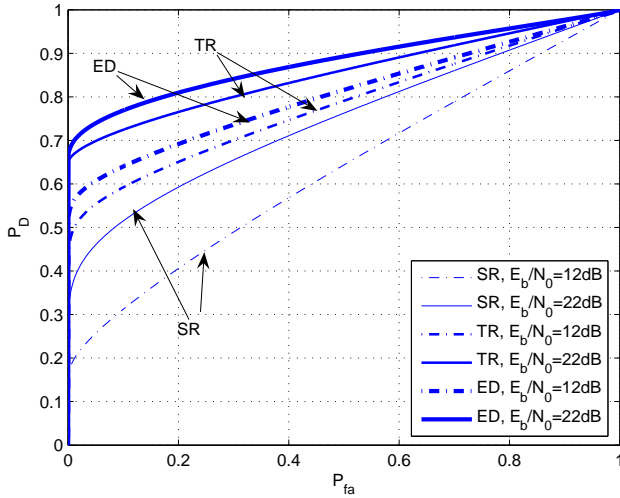


Fig. 8. ROC (theory) for different transceiver types and in the presence of timing offsets ($N_s = 1$, $M = 8$).

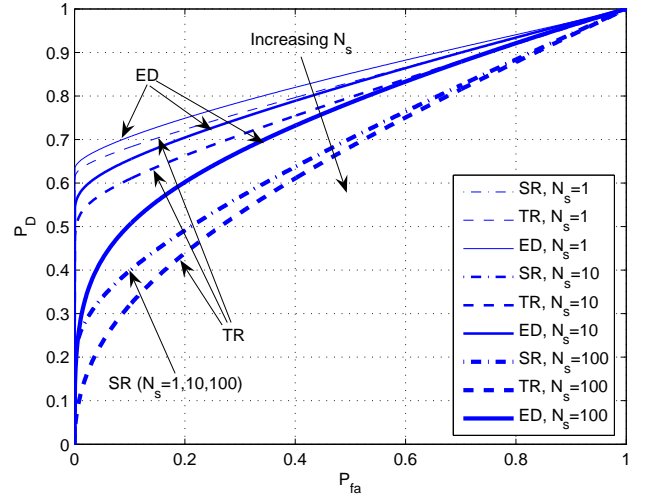


Fig. 10. ROC (theory) for different transceiver types and in the presence of timing offsets for $N_s = 1, 10, 100$ ($M = 8$, $N_{\text{symb}} = 1$, $E_b/N_0 = 17\text{dB}$).

degradations are observed in the performances of TR and ED (see Fig. 10).

B. Multipath Channel Simulations

Effect of window length for MESS on timing error are investigated in Fig. 11 through Fig. 15. It is seen that regardless of the window length N_w , SR has a worse performance compared to ED and TR due to undersampled signal and the energy collection characteristics. On the other hand, Fig. 14 and Fig. 15 show that optimal window length is around 30ns, which is on the order of delay spread of the channel. The E_b/N_0 values for CM2 are selected higher than CM1 as CM2 hits the error floor at higher E_b/N_0 .

Note that these results do not contradict with the results presented in [14] (where SR outperforms ED) due to two

important reasons. First, in [14], multiple acquisition frames are considered, where SR has better characteristics over ED and TR. Second (and more important) reason is that we consider the average timing error of the peak with respect to the leading edge, assuming the presence of the signal. As implied by Fig. 4b, when there is a random timing offset within the first energy sample, the delay between the peak is larger on the average for SR compared to TR and ED. Therefore, regardless of the detection performance of SR, its mean absolute error (MAE) may be worse compared to other two schemes due to their correlation and energy collection characteristics.

The MAE of the TOA estimates for the techniques that require *a-priori* channel knowledge are presented in Fig. 16 for the ED (CM1, $T_b = 4\text{ns}$). The Bayesian estimation is obtained using the histograms of the signal energies within first $N_e = 25$ blocks. While it yields a lower bound at high

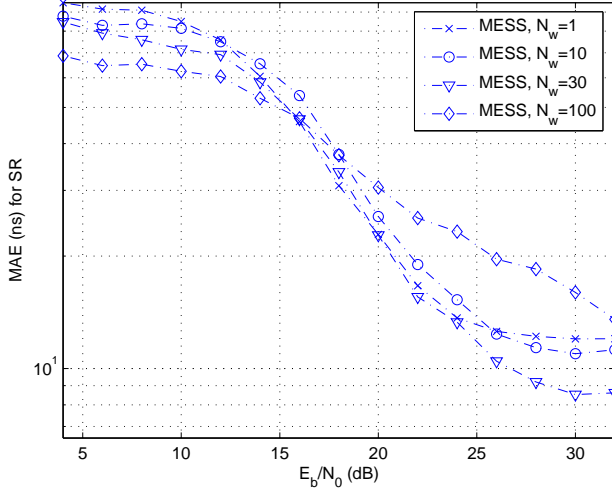


Fig. 11. MAE when using MESS and SR (CM1, $t_s = T_c = T_b = 1$ ns).

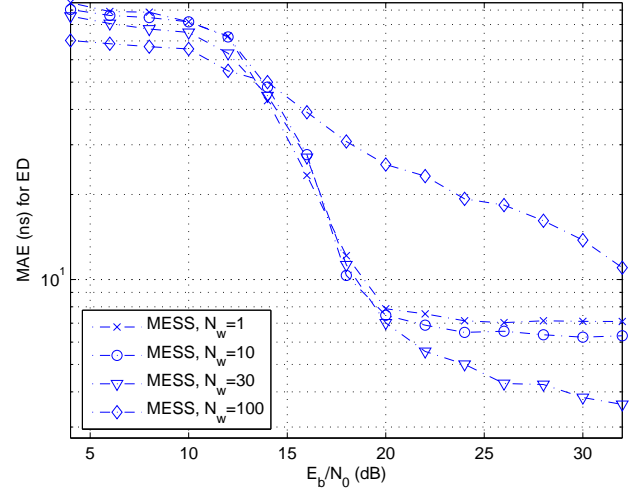


Fig. 13. MAE when using MESS and ED (CM1, $t_s = T_c = T_b = 1$ ns).

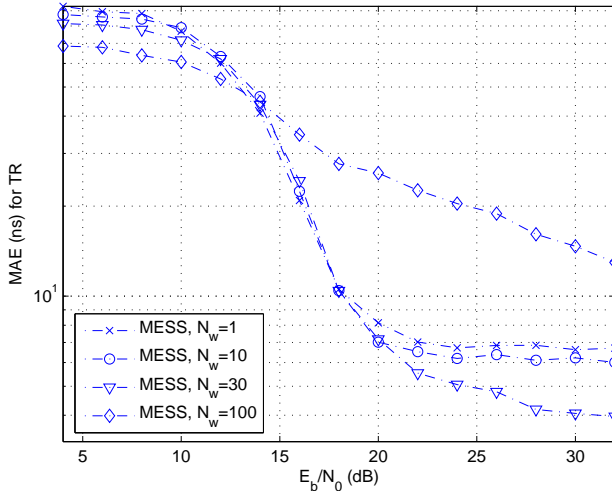


Fig. 12. MAE when using MESS and TR (CM1, $t_s = T_c = T_b = 1$ ns).

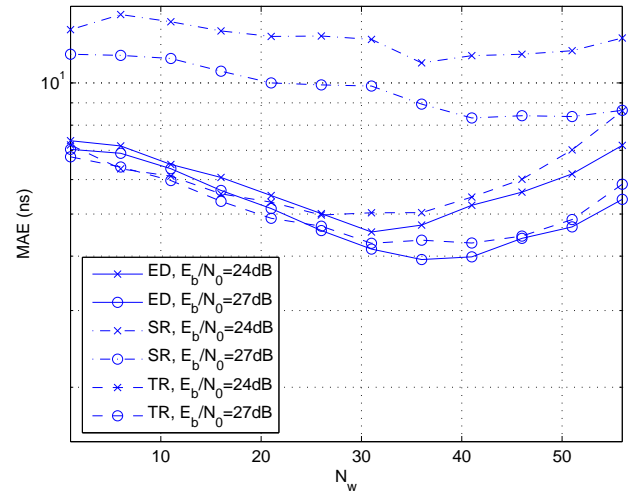


Fig. 14. MAE with respect to N_w for $E_b/N_0 \in \{24, 27\}$ dB for different transceivers (CM1, $t_s = T_b = 1$ ns).

E_b/N_0 , the Bayesian estimate is not as good at low E_b/N_0 . This may be explained with the fact that \mathcal{E}_m are assumed uncorrelated as discussed in Section IV-C. Also, small number of samples available (which may be insufficient to be modeled via the PDFs), the mismatch between the PDF and current realization (which may change slightly due to random timing offsets), or the inaccuracy of the Gaussian approximation of Chi-square statistics may be the other reasons affecting the optimality of Bayesian estimator. On the other hand, it is seen that W_2 MESS significantly outperforms MES, and has a reasonably low complexity, requiring power delay profile of the channel. Also, the four times decrease in the sampling rate yields a 1ns increase in the error floor for the performance of MES (to be compared with Fig. 13 for $N_w = 1$).

VI. CONCLUSION

In this paper, timing estimation for IR-UWB systems is analyzed for different transceiver types. Theoretical expres-

sions for peak selection error and leading edge detection performances are presented in AWGN channels with sampling rate constraints and by considering the energy collection characteristics of the transceivers. Processing gain is shown to be better exploited by SR compared to TR and ED. In multipath channels, optimal window length for peak selection is shown to be on the order of delay spread of the channel. Simulation results show that performance of peak selection can be enhanced by likelihood based methods that make use of channel information and noise statistics.

When an under-sampled signal is considered, SR, even though not observing non-coherent combining loss, is more susceptible to timing mismatches (and thus, sub-Nyquist sampling rate effects) compared to TR and ED. In order for stored-reference to have accurate timing and efficient energy capture, high sampling rates on the order of Nyquist rate are required. However, SR still has certain advantages even at low sampling rates. Considering the fact that the samples

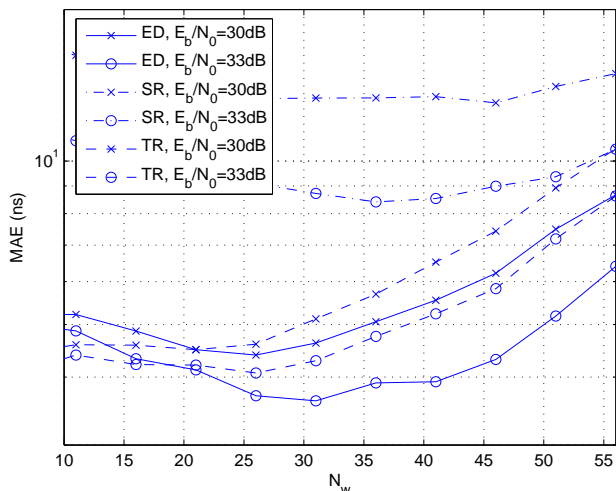


Fig. 15. MAE with respect to N_w for $E_b/N_0 \in \{30, 33\}$ dB for different transceivers (CM2, $t_s = T_b = 1$ ns).

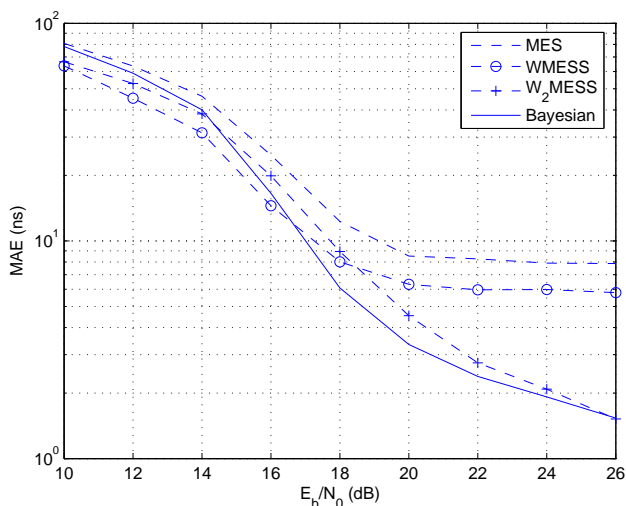


Fig. 16. Performances of different TOA estimators for ED (CM1, $t_s = T_b = 4$ ns).

are required to be averaged over a long preamble in order to achieve precision ranging requirements of wireless networks, SR is more beneficial as it does not observe non-coherent combining loss. Spectral mask and peak to average power ratio requirements of regulatory agencies may also enforce using multiple pulses to distribute the energy over time, which is in favor of SR.

REFERENCES

- [1] J.-Y. Lee and R. A. Scholtz, "Ranging in a dense multipath environment using an UWB radio link," *IEEE J. Select. Areas Commun.*, vol. 20, no. 9, pp. 1677–1683, Dec. 2002.
- [2] C. Mazzucco, U. Spagnolini, and G. Mulas, "A ranging technique for UWB indoor channel based on power delay profile analysis," in *Proc. IEEE Vehic. Technol. Conf. (VTC)*, Los Angeles, CA, Sep. 2004, pp. 2595–2599.
- [3] B. Denis, J. Keignart, and N. Daniele, "Impact of NLOS propagation upon ranging precision in UWB systems," in *Proc. IEEE Conf. Ultrawideband Syst. Technol. (UWBST)*, Reston, VA, Nov. 2003, pp. 379–383.

- [4] S. Gezici, Z. Sahinoglu, H. Kobayashi, and H. V. Poor, *Ultra Wideband Geolocation*. John Wiley & Sons, Inc., 2005, in *Ultrawideband Wireless Communications*.
- [5] A. Rabbachin and I. Oppermann, "Synchronization analysis for UWB systems with a low-complexity energy collection receiver," in *Proc. IEEE Conf. Ultrawideband Syst. Technol. (UWBST)*, Kyoto, Japan, May 2004, pp. 288–292.
- [6] K. Yu and I. Oppermann, "Performance of UWB position estimation based on time-of-arrival measurements," in *Proc. IEEE Conf. Ultrawideband Syst. Technol. (UWBST)*, Kyoto, Japan, May 2004, pp. 400–404.
- [7] R. Fleming, C. Kushner, G. Roberts, and U. Nandiwada, "Rapid acquisition for ultra-wideband localizers," in *Proc. IEEE Conf. Ultrawideband Syst. Technol. (UWBST)*, Baltimore, MD, May 2002, pp. 245–249.
- [8] I. Guvenc and Z. Sahinoglu, "Multiscale energy products for TOA estimation in IR-UWB systems," in *Proc. IEEE Global Telecommun. Conf. (GLOBECOM)*, St. Louis, MO, Dec. 2005.
- [9] —, "TOA estimation with different IR-UWB transceiver types," in *Proc. IEEE Int. Conf. UWB (ICU)*, Zurich, Switzerland, Sept. 2005, pp. 426–431.
- [10] W. Chung and D. Ha, "An accurate ultra wideband (UWB) ranging for precision asset location," in *Proc. IEEE Conf. Ultrawideband Syst. Technol. (UWBST)*, Reston, VA, Nov. 2003, pp. 389–393.
- [11] J. Yu and Y. Yao, "Detection performance of time-hopping ultrawideband LPI waveforms," in *Proc. IEEE Sarnoff Symp.*, Princeton, New Jersey, Apr. 2005, pp. 137–140.
- [12] M. Dawood and R. M. Narayanan, "Receiver operating characteristics for the coherent UWB random noise radar," *IEEE Trans. Aerospace and Electronic Syst.*, vol. 37, no. 2, pp. 586–594, April 2001.
- [13] Z. Tian and B. M. Sadler, "Weighted energy detection of ultrawideband signals," in *Proc. IEEE Signal Processing Workshop on Advances in Wireless Communications (SPAWC)*, New York, NY, June 2005.
- [14] L. Reggiani and G. M. Maggio, "Rapid search algorithms for code acquisition in UWB impulse radio communications," *IEEE J. Select. Areas Commun.*, vol. 23, no. 5, pp. 898–908, May 2005.
- [15] Z. Tian and G. B. Giannakis, "A GLRT approach to data-aided timing acquisition in UWB radios – Part I: Algorithms," *IEEE Trans. Wireless Commun.*, 2005 (to appear).
- [16] —, "A GLRT approach to data-aided timing acquisition in UWB radios – Part II: Training sequence design," *IEEE Trans. Wireless Commun.*, 2005 (to appear).
- [17] Z. Tian and V. Lottici, "Efficient timing acquisition in dense multipath for UWB communications," in *Proc. IEEE Vehic. Technol. Conf. (VTC)*, vol. 2, Orlando, FL, Oct. 2003, pp. 1318–1322.
- [18] I. Guvenc and Z. Sahinoglu, "Threshold-based TOA estimation for impulse radio UWB systems," in *Proc. IEEE Int. Conf. UWB (ICU)*, Zurich, Switzerland, Sept. 2005, pp. 420–425.
- [19] R. A. Scholtz and J. Y. Lee, "Problems in modeling UWB channels," in *Proc. IEEE Asilomar Conf. Signals, Syst. Computers*, vol. 1, Monterey, CA, Nov. 2002, pp. 706–711.
- [20] M. H. Chung and R. A. Scholtz, "Comparison of transmitted- and stored-reference systems for ultra-wideband communications," in *Proc. IEEE Military Commun. Conf. (MILCOM)*, Monterey, CA, Oct. 2004.
- [21] A. Papoulis, *Probability, Random Variables, and Stochastic Processes*. New York: McGraw-Hill, 1991.
- [22] I. Guvenc, Z. Sahinoglu, A. F. Molisch, and P. Orlik, "Non-coherent TOA estimation in IR-UWB systems with different signal waveforms," in *Proc. IEEE Int. Workshop on Ultrawideband Networks (UWBNETS)*, Boston, MA, October 2005, (invited paper).
- [23] A. F. Molisch, K. Balakrishnan, C. C. Chong, S. Emami, A. Fort, J. Karedal, J. Kunisch, H. Schantz, U. Schuster, and K. Siwiak, "IEEE 802.15.4a channel model - final report," Sept., 2004. [Online]. Available: <http://www.ieee802.org/15/pub/TG4a.html>
- [24] J. G. Proakis, *Digital Communications*, 4th ed. New York: McGraw-Hill, 2001.
- [25] S. M. Kay, *Fundamentals of Statistical Signal Processing: Detection Theory*. Upper Saddle River, NJ: Prentice Hall, Inc., 1998.